IEEE Access
Multidisciplinary | Rapid Review | Open Access Journal

Received March 3, 2018, accepted April 8, 2018, date of publication April 11, 2018, date of current version May 2, 2018.

Digital Object Identifier 10.1109/ACCESS.2018.2825678

Disturbance Observer Based Fuzzy Sliding Mode Control of PV Grid Connected Inverter

YUNKAI ZHU AND JUNTAO FEI, (Senior Member, IEEE)
Jiangsu Key Laboratory of Power Transmission and Distribution Equipment Technology, College of IoT Engineering, Hohai University, Nanjing 213022, China
Corresponding author: Juntao Fei (jtfei@hhu.edu.cn)

This work was supported in part by the Natural Science Foundation of Jiangsu Province under Grant BK20171198 and in part by the Fundamental Research Funds for the Central Universities under Grant 2017B20014 and Grant 2017B21214.

ABSTRACT In this paper, a disturbance observer-based fuzzy sliding mode control (DOBFSMC) strategy is proposed for a single-phase PV grid-connected inverter. In the fact that the uncertainties caused by the inverter component parameter variations and the changes of climatic conditions may seriously affect the control performance of the inverter, a disturbance observer is designed to estimate these disturbances in real time and a sliding mode controller designed with the output information of the disturbance observer is employed to control the output voltage of the DC–AC inverter, and a fuzzy system is used to approximate the upper bound of the observation error between the actual disturbance and its observation value in order to improve the performance of the control system. The inverter has strong robustness since the disturbances can be adaptively compensated, and the chattering is greatly reduced since the switching gain can be very small as the upper bound of observation error is estimated by the fuzzy system. Finally, simulation results verify the effectiveness of the proposed method and demonstrate it can work reliably under different conditions.

INDEX TERMS PV grid-connected inverter, disturbance observer, fuzzy-sliding mode control.

I. INTRODUCTION

In recent years, with the depletion of traditional primary energy, the exploitation of renewable energy such as solar energy and wind energy is urgently required. More and more scholars have devoted themselves to the research of PV generation technology [1], [2]. The inverter is indispensable since the DC power generated by PV cells need to be converted into AC power to be used. The transformerless inverter is widely used for the characteristic of light weight, small size and low cost [3], [4]. Normally, a two-stage single-phase PV grid connected inverter without isolation transformer is mainly composed of DC-DC converter and DC-AC inverter. The maximum power point tracking (MPPT) is usually accomplished in the DC-DC part in order to improve the efficiency of PV system and in the DC-AC part, the DC power is turned into AC power to inject to the grid. Common Maximum Power Point Tracking (MPPT) schemes such as constant voltage tracking (CVT) [5], incremental conductance (INC) method [6], disturbance observation method [7] are proposed. CVT which has low accuracy and poor reliability is just a means of voltage stabilizing rather than MPPT. The conductance increment method and the perturbation observation method may oscillate near the maximum power point (MPP), normally an adaptive step can achieve better performance.

Plenty of strategies are available to control the inverter. Evran [8] presented a two-stage inverter topology for single-phase grid-connected PV applications by designing a high gain DC-DC converter to connect the low-voltage PV panel to the grid and a plug-in repetitive controller to reduce the grid current THD. Xiao *et al*. [9] employed two DC-bus voltage regulators with different references for a grid-connected PV inverter operating in both normal grid voltage mode and low grid voltage mode. An additional DC-bus voltage regulator paralleled with MPPT controller is used to guarantee the reliability of the low voltage ride-through of the inverter. Cecati etc. Reference [10] proposed a single-phase H-bridge multilevel converter for PV systems governed by a new integrated fuzzy controller..

As an effective way of observing external disturbances in systems, the estimation principle of disturbance observer has recently been studied [11]. Kim and Kim [12] designed a disturbance observer to observe the grid voltages in the stationary reference frame using the current measurements and reference signals. Ozsoy *et al.* [13] proposed a disturbance observer- based decoupled current approach for a grid-connected inverter under unbalanced network conditions. Sliding mode control (SMC) ([14]–[16]) is a nonlinear control strategy, whose basic feature is its

discontinuity. There are some scholars applied SMC to control the grid-connected inverter [17]–[21], [26]. Merabet *et al*. [20] employed a sliding mode compensator into the inverter to enhance its robustness to uncertainties. The feedback linearizing control schemes are developed from the grid model at the inverter side and the DC-link model at the DC-DC converter side. Kumar *et al*. [21] presented a sliding mode algorithm to control the active and reactive powers flowing into the grid. Fei and Zhu [22] proposed an adaptive fuzzy-sliding mode control scheme which combines sliding mode control and fuzzy logic to control the inverter. In order to obtain the properties of finite time convergence, Zhu and Fei [23] presented a fast terminal sliding mode control with fuzzy- neural network to compensate the system uncertainties. In [24], a sliding mode control approach is used for achieving maximum power tracking control of a solar-PV array. The Lyapunov function-based control approach is designed and modeled for the DC-AC inverter to serve the functions of an active power injection to the grid. It is known that the switching term in the SMC which is designed to compensate the impact of the uncertainties is generally large in order to ensure the stability of the system, causing chattering problem in SMC. One effective scheme to reduce the chattering is to decrease the switching gain as more as possible.

In this paper, an INC scheme with adaptive step is adopted to track the MPP, a fuzzy sliding mode control strategy based on disturbance observer is proposed for a DC-AC inverter. The disturbance observer is presented to estimate the system uncertainties in real time. A sliding mode controller designed with the output information of the disturbance observer is employed to control the output voltage of the DC-AC inverter, and a fuzzy system is used to approximate the upper bound of the observation error in order to improve the performance of the control system. The innovation and characteristic of this paper are summarized as follows:

(1) The disturbance observer is designed to estimate the system uncertainties in real time so that the system uncertainties can be effectively compensated which enhance the robustness of the system. Therefore it is convenient to control the inverter for the disturbances can be adaptively estimated;

(2) Fuzzy control and SMC are combined to achieve better performance. The system has strong robustness for the sliding mode is designed independently without the information of the system nonlinearities;

(3) Fuzzy system is adopted to estimate the upper bound of the observation error in real time as a result the switching gain can be adaptively adjusted, which greatly reduce the chattering in the sliding mode.

This paper is organized as follows: Sec.II presents a model of the two-stage single-phrase PV grid-connected system. In Sec.III, an INC scheme with adaptive step is given to track the MPP. In Sec.V, a disturbance observer based fuzzy sliding mode controller for the inverter is presented. Simulation studies are presented in Sec.V to verify the effectiveness of the proposed control strategies. Finally, conclusions are drawn in Sec.VI.

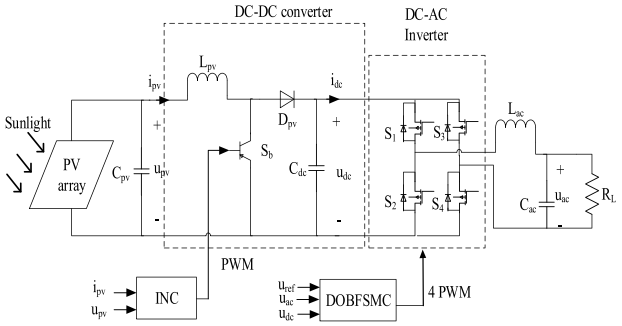

FIGURE 1. Single-phrase PV grid-connected system.

II. SYSTEM DESCRIPTION

As shown in Fig.1, a typical two-stage PV grid-connected system without isolation transformer mainly consists of a PV module, a DC-DC converter and a DC-AC inverter [9]. The boost chapter consists of a controllable power switch S_b, an inductor L_{pv}, a capacitor C_{dc} and a diode D_{pv}, DC-AC inverter consists of four controllable power switches, L_{ac} and C_{ac} are the inductor and capacitor of the filter in AC side, R_L is the load in grid side. The PV module converts solar energy into direct current and DC-DC converter enlarges the output voltage of the PV module since it is usually relatively small, the DC-AC inverter converts the enlarged DC power into AC power and injects it to the grid through a filter.

In this part, we are going to establish the mathematical model of the inverter. Before establishing the mathematical expression of the inverter, we make the following assumptions: $S_1 - S_4$ are all ideal switches with zero on-resistance, the dead time and capacitance and inductance effect can be ignored. The parasitic resistance of inductor L_{ac} and capacitor C_{ac} is small enough to be ignored.

According the KVL and KCL, the following formula can be derived

While S_1, S_4 are on,

$$\begin{cases} C_{ac}\dfrac{du_{ac}}{dt} + \dfrac{1}{R_L}u_{ac} - i_{ac} = 0 \\ L_{ac}\dfrac{di_{ac}}{dt} - u_{dc} + +u_{ac} = 0 \end{cases} \tag{1}$$

While S_2, S_3 are on

$$\begin{cases} C_{ac}\dfrac{du_{ac}}{dt} + \dfrac{1}{R_L}u_{ac} - i_{ac} = 0 \\ L_{ac}\dfrac{di_{ac}}{dt} + u_{dc} + u_{ac} = 0 \end{cases} \tag{2}$$

where u_{dc} is the voltage of the inverter in the DC side, u_{ac} and i_{ac} are the voltage and current in the AC side respectively.

Assuming D is the duty cycle of S_1 and S_4, then that of S_2 and S_3 is 1-D.

Combining (1) and (2) derives

$$L_{ac}\frac{di_{ac}}{dt} = (2D-1)u_{dc} - u_{ac} \tag{3}$$

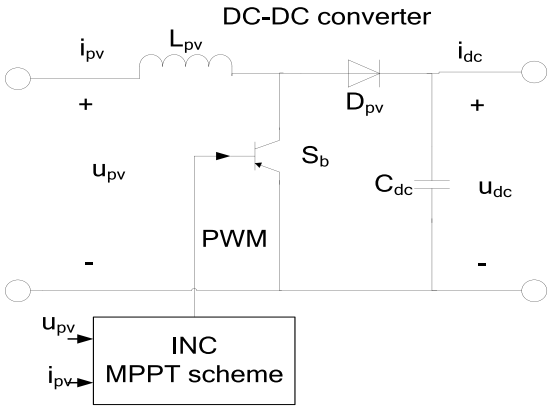

FIGURE 2. DC-DC converter.

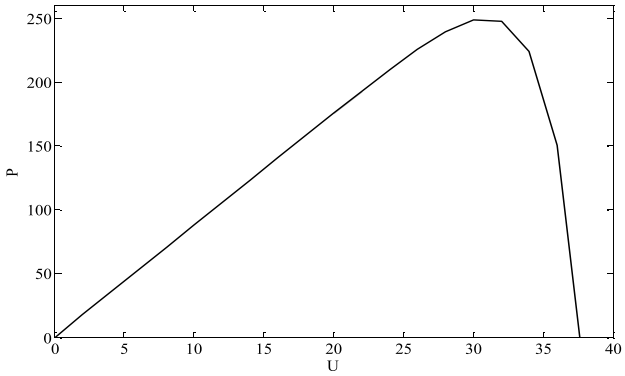

FIGURE 3. P-U characteristics of PV module.

$$C_{ac}\frac{du_{ac}}{dt} = i_{ac} - \frac{1}{R_L}u_{ac} \tag{4}$$

Taking derivative of (4) gives

$$\frac{d^2u_{ac}}{dt^2} = \frac{1}{C_{ac}}\frac{di_{ac}}{dt} - \frac{1}{R_LC_{ac}}\frac{du_{ac}}{dt} \tag{5}$$

Appling (3) into (5) derives

$$\frac{d^2u_{ac}}{dt^2} = -\frac{1}{R_LC_{ac}}\frac{du_{ac}}{dt} - \frac{1}{L_{ac}C_{ac}}u_{ac} + \frac{2D-1}{L_{ac}C_{ac}}u_{dc} \tag{6}$$

Since u_{ac} and its derivative as well as u_{dc} can be measured, so the equation (6) has practical significance. In practical applications, the inverter is affected by parameter variations and external disturbances, as a result, the expression of (6) cannot describe the actual model of the inverter and need to be modified. Considering the nonlinearities in the inverter model, (6) can be rewritten as

$$\frac{d^2u_{ac}}{dt^2} = -(\frac{1}{R_LC_{ac}} + \Delta_1)\frac{du_{ac}}{dt} - (\frac{1}{L_{ac}C_{ac}} + \Delta_2)u_{ac} + (\frac{2D-1}{L_{ac}C_{ac}} + \Delta_3)u_{dc} \tag{7}$$

where Δ_1 and Δ_2 is the parameters variations, Δ_3 is the uncertainties caused by u_{dc}.

Define $d(t) = -\Delta_1\frac{du_{ac}}{dt} - \Delta_2u_{ac} - \Delta_3u_{dc}$ as the system disturbances, then the mathematical expression of the inverter can be described as (8)

$$\frac{d^2u_{ac}}{dt^2} = -\frac{1}{R_LC_{ac}}\frac{du_{ac}}{dt} - \frac{1}{L_{ac}C_{ac}}u_{ac} + \frac{2D-1}{L_{ac}C_{ac}}u_{dc} + d(t) \tag{8}$$

where d(t) is a bounded lumped parameter which represents the uncertainties caused by environment condition variations, parameters variations and the modeling error of the DC-AC inverter.

III. DC-DC CONVERTER AND MPPT STRATEGY

The presented DC-DC converter shown in Fig.2 is a boost chapter which consists of a controllable power switch S_b, an inductor L_{pv}, a capacitor C_{dc} and a diode D_{pv}. Assuming that the inductance L_{pv} and capacitance C_{dc} of the converter are large enough that the current i_{pv} and the voltage u_{dc} can keep constant during the switch S_b on and off time. Defining $D_b(0 < D_b < 1)$ as the duty cycle of S_b, as the fact that the energy accumulated by the L_{pv} in one cycle is equal to the energy it released, we have

$$u_{pv} \cdot i_{pv} \cdot D_b = (u_{dc} - u_{pv}) \cdot i_{pv} \cdot (1 - D_b) \tag{9}$$

Since i_{pv} can be regarded as constant as assumed before, (9) can derives

$$u_{pv} = (1 - D_b)u_{dc} \tag{10}$$

From (10) it can be concluded that when u_{dc} keeps constant, u_{pv} and D_b vary contrarily, hence we can get suitable u_{pv} that make the PV system working with maximum power by controlling D_b.

The MPPT of PV system is necessary in order to improve the efficiency of the PV system since the PV module is susceptible to environmental factors such as irradiance level and surrounding temperature. The P-U characteristics of PV module are shown in Fig. 3.

It can be found from Fig.3 that the peak point of the curve is the MPP satisfying

$$\frac{dP}{dU_{pv}} = \frac{d(U_{pv}I_{pv})}{U_{pv}} = I_{pv} + U_{pv}\frac{dI_{pv}}{dU_{pv}} = 0 \tag{11}$$

Rewriting it as

$$\frac{dI_{pv}}{dU_{pv}} = -\frac{I_{pv}}{U_{pv}} \tag{12}$$

In numerical algorithm, dI_{pv} and dU_{pv} can be modified as

$$\begin{cases} dI_{pv} = I_{pv}(k) - I_{pv}(k-1) \\ dU_{pv} = U_{pv}(k) - U_{pv}(k-1) \end{cases} \tag{13}$$

It is known from (10) that the PV output voltage U_{pv} and D_b vary conversely. So we can get the suitable U_{pv} which makes the PV system working at the MPP by adjusting D_b.

The essence of searching the MPP by INC scheme is to search the working point that satisfies the equation (11).There will be three situations in the process of INC scheme:

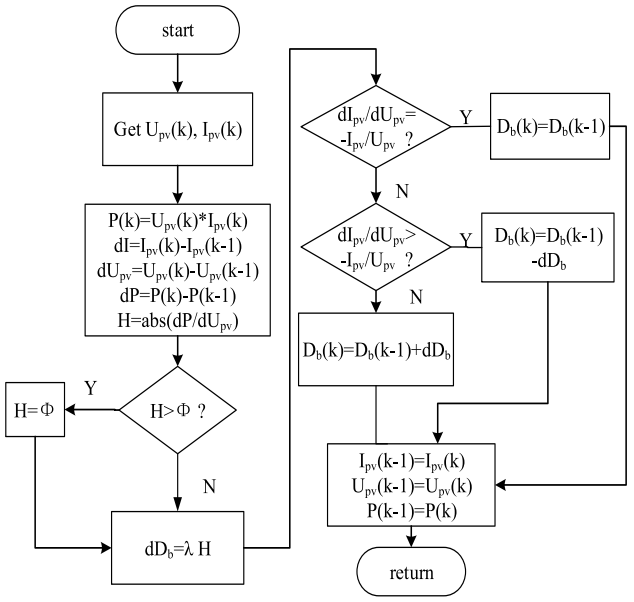

FIGURE 4. INC method with adaptive step.

1. When $dI_{pv}/dU_{pv} > -I_{pv}/U_{pv}$, that is $dP/dU_{pv} > 0$, the current working point locates on the left side of the MPP, it need to reduce the D_b to increase U_{pv},

$$D_b(k) = D_b(k-1) - dD_b;$$

2. When $dI_{pv}/dU_{pv} < -I_{pv}/U_{pv}$, that is $dP/dU_{pv} < 0$, the current working point locates on the right side of the MPP, it need to increase D_b to decrease U_{pv}.

$$D_b(k) = D_b(k-1) + dD_b$$

3. When $dI_{pv}/dU_{pv} = -I_{pv}/U_{pv}$, that is $dP/dU_{pv} = 0$, the current working point is the MPP.

Choosing the adaptive step size as $\lambda \times \left|dp/dU_{pv}\right|$, where λ is a positive constant, the iteration algorithm is expressed as (14)

$$D_b(k) = D_b(k-1) \pm \lambda \left|\left|dp/dU_{pv}\right|\right| \tag{14}$$

The sign in (14) is determined by the working point of the PV system. Detailed strategies are shown in Fig.4 where Φ is a threshold parameter to prevent too large step.

IV. DISTURBANCE OBSERVER BASED FUZZY SLIDING MODE CONTROL

A. DISTURBANCE OBSERVER DESIGN

From part 2, it is known that the inverter may face the challenge of unknown disturbances. In order to compensate the impact of those nonlinearities, a disturbance observer is designed.

For the inverter model described by (8), the system uncertainties can be expressed as

$$d = \ddot{u}_{ac} + \frac{1}{R_L C_{ac}}\dot{u}_{ac} + \frac{1}{L_{ac}C_{ac}}u_{ac} - \frac{2D-1}{L_{ac}C_{ac}}u_{dc} \tag{15}$$

Defining $\hat{d}$ as the output of the observer, updating the observation value by using the error between $\hat{d}$ and d as shown in (16) [25]

$$\begin{aligned}\dot{\hat{d}} &= r(d-\hat{d}) \\ &= r(\ddot{u}_{ac} + \frac{1}{R_L C_{ac}}\dot{u}_{ac} + \frac{1}{L_{ac}C_{ac}}u_{ac} - \frac{2D-1}{L_{ac}C_{ac}}u_{dc} - \hat{d})\end{aligned} \tag{16}$$

where $\dot{\hat{d}}$ is the derivative of $\hat{d}$, representing the varying trend of $\hat{d}$, r is a constant positive.

Eq. (16) represents a simple observer but it requires the information of the second derivative of the AC side voltage. In practical applications, it is difficult to obtain the acceleration signal by differentiating the velocity signal since there exist observation noises. Therefore, a new observer is established by introducing an instrumental variable as $z = \hat{d} - r \cdot \dot{u}_{ac}$, whose derivative is represented as (17)

$$\dot{z} = \dot{\hat{d}} - r \cdot \ddot{u}_{ac} = r(\frac{1}{R_L C_{ac}}\dot{u}_{ac} + \frac{1}{L_{ac}C_{ac}}u_{ac} - \frac{2D-1}{L_{ac}C_{ac}}u_{dc} - \hat{d}) \tag{17}$$

Then a disturbance observer is obtained as

$$\begin{cases}\dot{z} = r(\frac{1}{R_L C_{ac}}\dot{u}_{ac} + \frac{1}{L_{ac}C_{ac}}u_{ac} - \frac{2D-1}{L_{ac}C_{ac}}u_{dc} - \hat{d}) \\ \hat{d} = z + r \cdot \dot{u}_{ac}\end{cases} \tag{18}$$

It can be observed from (18) that the presented observer does not need the information of the second derivative of u_{ac}, which means the practicability for application. Furthermore, the observation error can be exponentially convergent.

Remark1: Normally, for constant or slow disturbance, $\dot{d}$ is assumed to be zero. Defining the observation error as $\tilde{d} = d - \hat{d}$ Then

$$\dot{\tilde{d}} = \dot{d} - \dot{\hat{d}} = -\dot{\hat{d}} = -r \cdot \tilde{d} \tag{19}$$

Rewriting it as $\dot{\tilde{d}} + r \cdot \tilde{d} = 0$

It can be derived that

$$\tilde{d}(t) = \tilde{d}(t_0)e^{-rt} \tag{20}$$

where $\tilde{d}(t_0)$ is the initial error. It can be concluded from (20) that $d(t)$ is exponentially convergent and the convergent speed can be designed by adjusting r.

B. DISTURBANCE OBSERVER BASED SLIDING MODE CONTROL

Defining the tracking error between the inverter output voltage and the grid reference voltage as $e = u_{ac} - u_{ref}$, where u_{ac} is the output voltage of the inverter, u_{ref} represents the grid reference voltage.

Selecting a sliding surface as

$$s = c \cdot e + \dot{e} \tag{21}$$

where c is a constant positive, e is the voltage tracking error, $\dot{e}$ is the derivative of e.

Designing the control law as

$$D = \frac{1}{2}[1 + \frac{L_{ac}C_{ac}}{u_{dc}}(\ddot{u}_{ref} + \frac{1}{R_L C_{ac}}\dot{u}_{ac} + \frac{1}{L_{ac}C_{ac}}u_{ac} - c\dot{e} - \hat{d} - ks - \eta sgn(s))] \quad (22)$$

where k is a positive constant, $\hat{d}$ is the observation value of the disturbances, η is the upper bound of observation error $\tilde{d}$, which satisfies $\eta >= \left|\tilde{d}\right|_{\max}$.

Theorem 1: The system using disturbance observer based sliding mode control (DOBSMC) scheme with the control law determined by (22) where $\hat{d}$ is given in (18) can be asymptotically stable.

Proof: Taking the derivative of s with respect to time yields

$$\begin{aligned}\dot{s} &= c\dot{e} + \ddot{e} = c\dot{e} + \ddot{u}_{ac} - \ddot{u}_{ref} \\ &= c\dot{e} - \ddot{u}_{ref} - \frac{1}{R_L C_{ac}}\dot{u}_{ac} - \frac{1}{L_{ac}C_{ac}}u_{ac} + \frac{2D-1}{L_{ac}C_{ac}}u_{dc} + d\end{aligned} \quad (23)$$

Applying the control law (22) to (23), we get

$$\dot{s} = d - ks - \eta sgn(s) \quad (24)$$

Selecting a Lyapunov function candidate as

$$V_1 = \frac{1}{2}s^2 + \frac{1}{2}\tilde{d}^2 \quad (25)$$

where s is the sliding mode function, $\tilde{d} = d - \hat{d}$ is the observation error.

Taking the derivative of (25) gives

$$\begin{aligned}\dot{V}_1 &= s\dot{s} + \tilde{d}\dot{\tilde{d}} = s\dot{s} - k\tilde{d}^2 = s(\tilde{d} - ks - \eta sgn(s)) - k\tilde{d}^2 \\ &= s\tilde{d} - ks^2 - \eta|s| - k\tilde{d}^2 \leq -(\eta - \tilde{d})|s| - ks^2 - k\tilde{d}^2 < 0\end{aligned} \quad (26)$$

V_1 is negative definite which guarantees the stability of the system. In practical applications, the observation error $\tilde{d}$ is time-varying, so the switching gain η that represented the upper bound of the observation error should also be time-varying because a too large value of η will cause large oscillation but a too small value cannot guarantee the stability of the system if η is set to a fixed value. Therefore, in nex section, a fuzzy system is introduced to approximate the upper bound of the observation error.

C. DISTURBANCE OBSERVER BASED FUZZY SLIDING MODE CONTROL

Form the analysis above, it is known that the switching gain η representing the upper bound of the observation error should be time-varying since d is time-varying and the observation error $\tilde{d}$ is time-varying. Hence a fuzzy system is adopted to approximate the upper bound of the observation error. The control block of DOBFSMC is shown in Fig.5.

Employing a fuzzy system to approximate η. By using strategy of singleton fuzzification, product inference and center-average defuzzification, the output of the fuzzy system is presented as

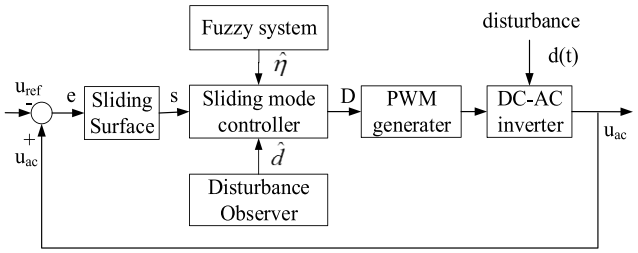

FIGURE 5. The control block of DOBFSMC.

$$\hat{\eta} = \frac{\sum w_i \times \mu_i}{\sum \mu_i} = w^T \xi \quad (27)$$

where $\hat{\eta}$ represents the estimated value of η, w is an adjustable vector that can update based on adaptive laws. ξ is a fuzzy basis function vector, and $\xi_i = \frac{\mu_i}{\sum \mu_i}$, i = 1,2,3.....m, where m is the number of membership functions.

Assumption1: According to the universal approximation principle, for any small positive number ε^* and a continuous function $\eta(t)$, there exists the optimal parameter w^* such that the output of the fuzzy system satisfies $\left|\eta(t) - w^{*T}\zeta\right| < \varepsilon^*$. Assuming that the observation error $\tilde{d}$ and its upper bound η satisfies $\eta - |\tilde{d}| > \varepsilon^*$.

Redesigning the control law as (28) by adopting fuzzy system described by (29) to estimate η, and replacing η in the control law (22) by $\hat{\eta}$

$$D = \frac{1}{2}[1 + \frac{L_{ac}C_{ac}}{u_{dc}}(\ddot{u}_{ref} + \frac{1}{R_L C_{ac}}\dot{u}_{ac} + \frac{1}{L_{ac}C_{ac}}u_{ac} - c\dot{e} - \hat{d} - ks - \hat{\eta}sgn(s))] \quad (28)$$

where k is a positive constant, $\hat{d}$ is the observation value of the disturbances, $\hat{\eta}$ is the output of fuzzy system, which represents the estimated value of the upper bound of observation error $\tilde{d}$.

Theorem 2: The system using DOBFSMC scheme with the control law (28) where $\hat{d}$ is given in (18) and $\hat{\eta}$ is the output of the fuzzy system with the update law presented by (29) can be asymptotically stable, the tracking error can converge to zero asymptotically.

The parameter w is updated by the adaptive law as(29)

$$\dot{w} = \rho\zeta|s| \quad (29)$$

where ρ is a positive constant, s is the sliding mode function, ζ is the fuzzy basis vector.

Proof: Defining $\tilde{w} = w - w^*$ as the error between w and the optimal parameter w^*. Choosing a positive definite function that determined by (30) as Lyapunov function

$$V = \frac{1}{2}s^2 + \frac{1}{2}\tilde{d}^2 + \frac{1}{2\rho}\tilde{w}^T\tilde{w} \quad (30)$$

Taking the derivative of (30) with respect to time yields

$$\dot{V} = s\dot{s} + \tilde{d}\dot{\tilde{d}} + \frac{1}{\rho}\tilde{w}^T\dot{\tilde{w}} \quad (31)$$

Appling the control law presented by (28) with the fuzzy system represented by (27) to (31) obtain

$$\begin{aligned}\dot{V} &= s\dot{s} + \tilde{d}\dot{\tilde{d}} + \frac{1}{\rho}\tilde{w}^T\dot{\tilde{w}} \\ &= s(\tilde{d} - ks - \hat{\eta}sgn(s)) - \tilde{d}^2 + \frac{1}{\rho}\tilde{w}^T\dot{\tilde{w}} \\ &= -ks^2 - \tilde{d}^2 - s\tilde{d} - w^T\zeta\,|s| + \frac{1}{\rho}\tilde{w}^T\dot{\tilde{w}} \end{aligned} \tag{32}$$

Using the adaptive law determined by (29), then

$$\begin{aligned}\dot{V} &= -ks^2 - \tilde{d}^2 + s\tilde{d} - w^T\zeta\,|s| + \tilde{w}^T\zeta\,|s| \\ &= -ks^2 - \tilde{d}^2 + s\tilde{d} - w^T\zeta\,|s| + (w^T - w^{*T})\zeta\,|s| \\ &= -ks^2 - \tilde{d}^2 + s\tilde{d} - w^{*T}\zeta\,|s| \end{aligned} \tag{33}$$

According to Assumption1, η satisfies $\left|\eta(t) - w^{*T}\zeta\right| < \varepsilon^*$, we have $\eta(t) - \varepsilon^* < w^{*T}\zeta < \eta(t) + \varepsilon^*$, then the following conclusion can be derived

$$\begin{aligned}\dot{V} &= -ks^2 - \tilde{d}^2 + s\tilde{d} - w^{*T}\zeta\,|s| \\ &< -ks^2 - \tilde{d}^2 + s\tilde{d} - (\eta - \varepsilon^*)\,|s| \\ &< -ks^2 - \tilde{d}^2 + \left|\tilde{d}\right|\,|s| - (\eta - \varepsilon^*)\,|s| \\ &= -ks^2 - \tilde{d}^2 - ((\eta - \varepsilon^*) - \left|\tilde{d}\right|)\,|s| \\ &= -ks^2 - \tilde{d}^2 - (\eta - \left|\tilde{d}\right| - \varepsilon^*)\,|s| < 0 \end{aligned} \tag{34}$$

$\dot{V}$ is negative definite ensures that V, s, $\dot{s}$ are all bounded,and $V(t) < V(0) < \infty$. Furthermore,

$\dot{V} < -ks^2 - \tilde{d}^2 - (\eta - \left|\tilde{d}\right| - \varepsilon^*)\,|s| < -ks^2$ implies that s is square integrable as $\int_0^t s^2 dt \le \frac{1}{k}(V(0) - V(t))$. Since $\dot{s}$ is bounded, according to the Barbalat lemma, it can be concluded that $s \to 0$ as $t \to \infty$, thereby $e \to 0$ as $t \to \infty$. In summary, The system using DOBSMC scheme with the control law (28) where $\hat{d}$ is given in (17), $\hat{\eta}$ is the output of the fuzzy system with the updated law presented by (29) can be asymptotically stable with zero tracking error.

Remark2: From Theorem 2, if d(t) varies slowly, the observer can catch this change in time and compensate it, if d(t) changes too fast or drastically, the observer can not keep up with the change as a result the observation error between the observation and the disturbance will increase, fortunately, the fuzzy system can compensate the observation error in real time, and the stability of the system can be guaranteed, so the system is not sensitive to the disturbance variation and parametric uncertainty. Therefore the proposed method is insensitive to parametric uncertainty.

Remark3: In practical applications, the initial duty cycle D obtained by the control law (28) may exceed the range of [0 1], so the saturation limit determined by (35) is applied in the experiment.

$$D = \begin{cases} 1 & if\ D > 1 \\ D & D \in [01] \\ 0 & if\ D < 0 \end{cases} \tag{35}$$

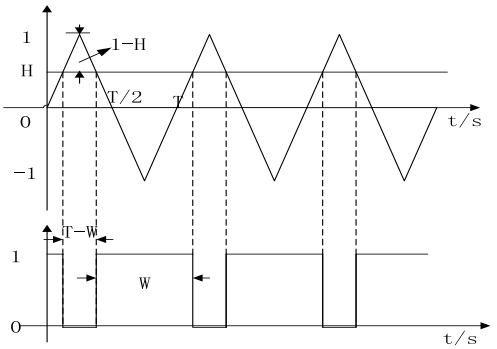

FIGURE 6. PWM signal modulation.

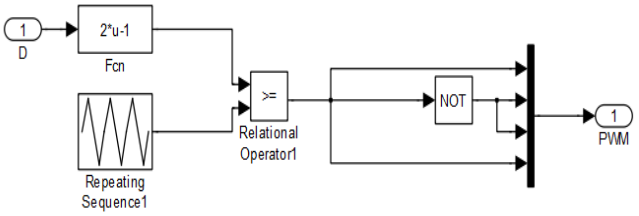

FIGURE 7. PWM generator.

The flowing words are going to introduce how to generate PWM signal with D duty cycle.

As shown in Fig.6, a horizontal line with height of H is compared with the triangle signal with amplitude of 1. If it is higher than the value of the triangle signal, logic-high is output, otherwise logic-low is generated. Thus, the PWM signal with different duty cycles is obtained by adjusting H.

Assuming that T is the cycle of the triangle signal, W is the width of logic-high of the PWM signal during time T. The duty cycle can be described as $\frac{W}{T}$. Geometric relationship from Fig.6 derives that $\frac{T-W}{T/2} = \frac{1-H}{1}$, furthermore we have $\frac{W}{T} = \frac{1+H}{2}$, which means the duty cycle of the generated PWM signal is $\frac{1+H}{2}$when the height of the horizontal signal is H.

Letting $D = \frac{1+H}{2}$, we get $H = 2D - 1$, which indicates that a PWM signal with a duty cycle of D can be generated by comparing horizontal signal height of $2D - 1$ and triangular wave height of 1.

Fig.7 shows the generation progress of the four PWM signals for $S_1 - S_4$, where the duty cycles of S_1 and S_4 are D, and that of S_2 and S_3 are $1 - D$.

V. SIMULATION STUDY

In order to verify the feasibility of the proposed strategies, a PV grid-connected system model is built in Simulink. The PV module is composed of two 250W photovoltaic components which are connected in series with the parameters as :$I_{sc} = 8.81AI_m = 8.36AV_m = 29.9VV_{oc} = 37.3V$. In MPPT strategy, $\Phi = 60$, $\lambda = 10^{-6}$. Simulation parameters are shown in Table 1. The experiment is implemented under the condition of environmental variations, load and

TABLE 1. Simulation parameters.

Parameters	Values	Parameters	Values
L_{pv}	$3\times10^{-4}H$	u_{ref}	$220\sqrt{2}\sin(100\pi t)$
C_{pv}	$10^{-3}F$	C_{ac}	$2.82\times10^{-5}F$
C_{dc}	$10^{-4}F$	L_{ac}	$0.048H$
λ	10^{-6}	c,k	$10^4, 5\times10^4$
ϕ	60	γ	10^{-3}
R_L	300Ω	ρ	10^{-3}

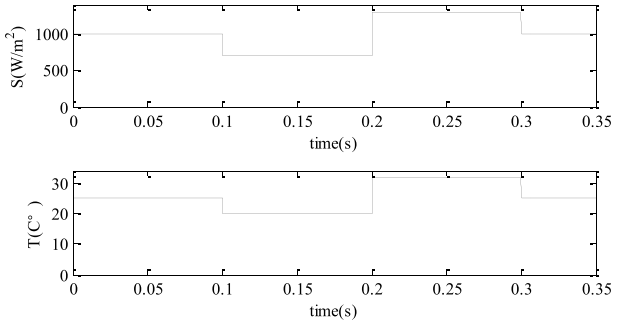

FIGURE 8. Variations of the environmental conditions.

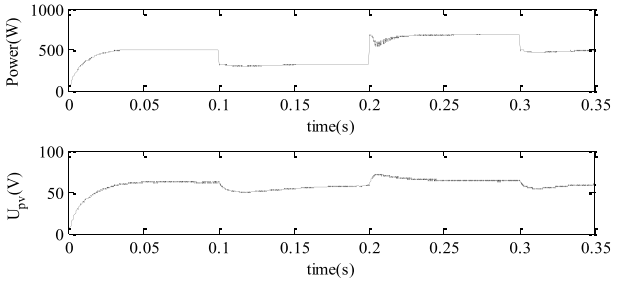

FIGURE 9. MPPT performance.

parameter variations and grid voltage fluctuation respectively, furthermore, comparison with SMC is accomplished.

A. ENVIRONMENTAL VARIATIONS

Since the PV module is sensitive to the environmental conditions. The variations of solar irradiance and temperature will directly affect the output of the PV modules, thereby affecting the output voltage of the inverter. In order to verify the adaptability of the proposed strategy to environmental variations, experiments are implemented.

As shown in Fig.8, the initial insolation level is set to be$1000W/m^2(100\%)$, and decrease to 880 W/m^2 (88%) when t = 0.2s, then increase to $950W/m^2$ (95%) at time 0.25s. The initial temperature is set to be 25 $°C$ (100%), at time 0.2s, it decrease to $21°C(84\%)$, and recover to $25°C(100\%)$ at time 0.3s. Fig.9 shows the MPPT performance, it can be seen that the proposed INC scheme can quickly trick the MPP without large chattering.

Fig.10 shows the voltage tracking progress of the inverter, it can be seen that the inverter output voltage can quickly track the reference voltage and keep consistent with it.

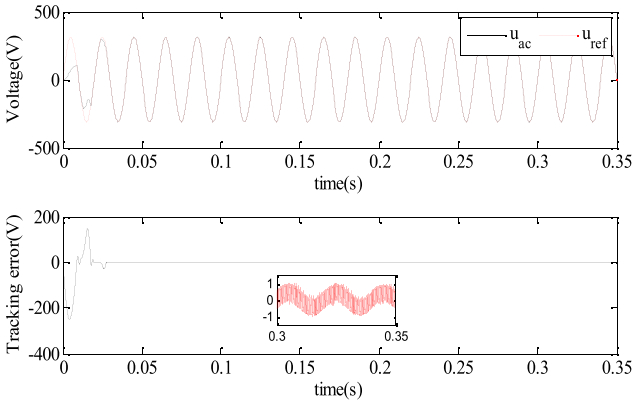

FIGURE 10. Voltage tracking performance of inverter.

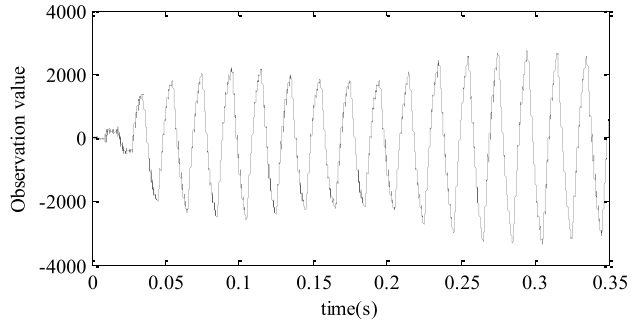

FIGURE 11. Disturbance estimation results.

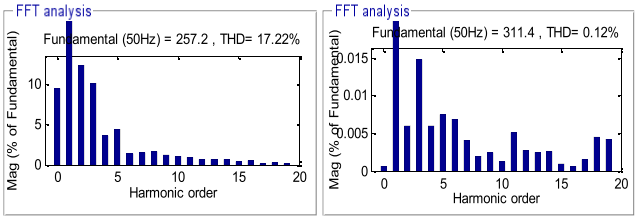

(a) (b)

FIGURE 12. FFT analysis of inverter output voltage. (a) Dynamic state. (b) Steady sate.

When the irradiance level and surrounding temperature vary, the inverter output voltage can always keep consistent with the reference voltage, showing the robustness to environmental variations. Furthermore, from the tracking error curve, it can be seen that the tracking error converges to zero asymptotically with the stability error bounded by $|e| < 0.8$.

Fig.11 depicts the disturbance estimation results. Fig.12 shows the THD of the output voltage of the inverter in dynamic and steady sate. When the inverter has not yet tracked the grid reference voltage, as shown in Fig.12 (a), the THD at time 0.04s is 21.57% indicating the serious distortion of the voltage. It can be seen from Fig.12 (b) that the THD is only 0.11% when t = 0.16s as the tracking progress to be stable after the output of inverter has tracked the reference voltage. The results above show the high power quality of the inverter using the proposed strategy.

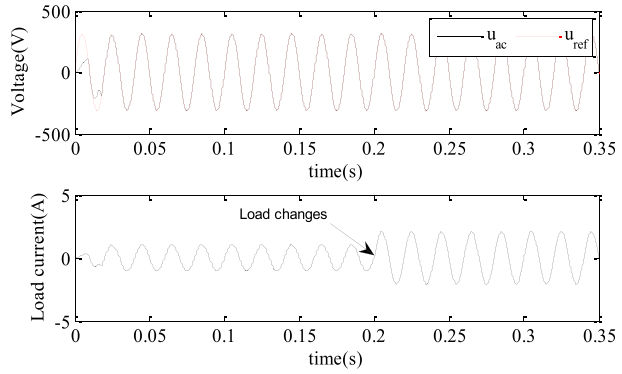

FIGURE 13. Performance under load and parameter variations.

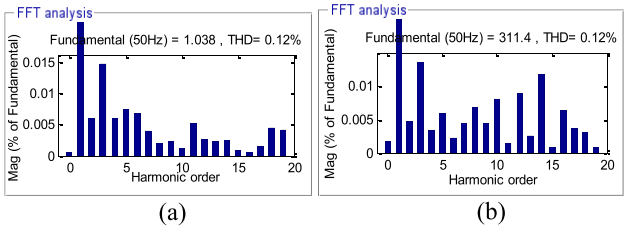

FIGURE 14. FFT analysis of load current.(a) Normal (b)Load and parameter variations.

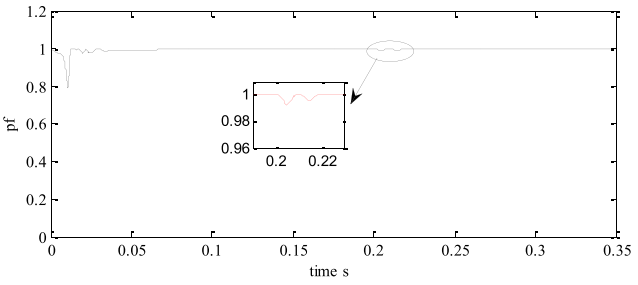

FIGURE 15. Power factor under load and parameter variations.

B. LOAD AND PARAMETER VARIATIONS

Parameter variations of the inverter system will increase the error between the established mathematical model of the inverter and its actual model, thereby seriously affecting the normal working of the inverter. Besides, the load mutation especially the connection of large inductive will also has impact on the inverter. This section aims to verify the robustness of the proposed control strategy to load fluctuation and parameter variations.

At time 0.2s, an additional capacitor with value of 10^{-6}F is added in paralleled with the capacitor C_{ac}, and a resistor-inductance load with inductance of 10^{-4}H and resistance of 300Ω is connected in parallel with the load.

Fig.13 shows the performance under load and parameter variations, as can be seen, the load current varies when the load changes, but its phase is always consistent with that of the reference voltage. Besides, the inverter output voltage still keep consistent with the reference voltage when the load and parameter vary, showing the insensitivity to these variations.

From Fig. 14(a), it can be seen that the THD of the load current in steady-state is 0.11% at time 0.16s, and its FFT analysis at t = 0.2s depicted in Fig.14 (b) shows that there is no obvious change in THD when the parameter and load vary. As shown in Fig.15, it can be seen that the power factor is slightly reduced and quickly restore to 1, indicating the high performance of the proposed strategy.

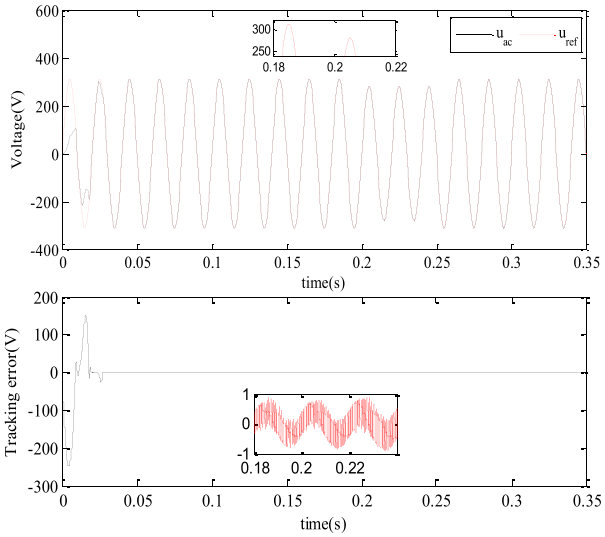

FIGURE 16. Tracking performance under grid voltage fluctuation.

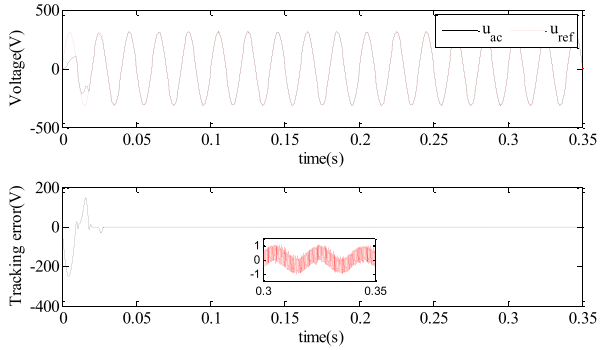

FIGURE 17. Voltage tracking performance using DOBFSMC.

C. VOLTAGE FLUCTUATION IN GRID SIDE

The grid voltage is not invariable because of the connection of plenty of nonlinear load and the injection of distributed power supplies. In order to verify the robustness of the proposed control strategy to the grid voltage fluctuation, the amplitude of the grid voltage is reduced to 280V (90%) at time 0.2s and recovers to 311V (100%) at time 0.24s. Fig.16 shows the performance of the inverter under grid voltage fluctuations. It can be seen that the inverter can quickly catch the variation of the grid voltage and adjust itself to track the reference voltage.

When the grid voltage returns to normal level, the inverter can also recover quickly, the output voltage of the inverter

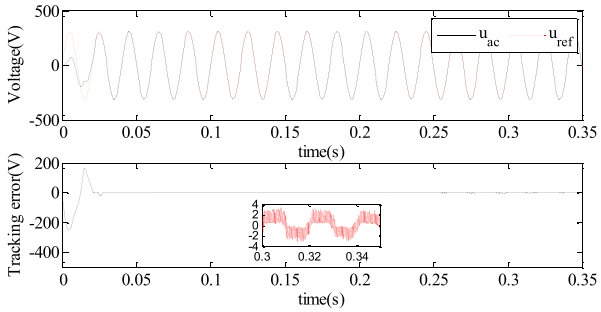

FIGURE 18. Voltage tracking performance using SMC.

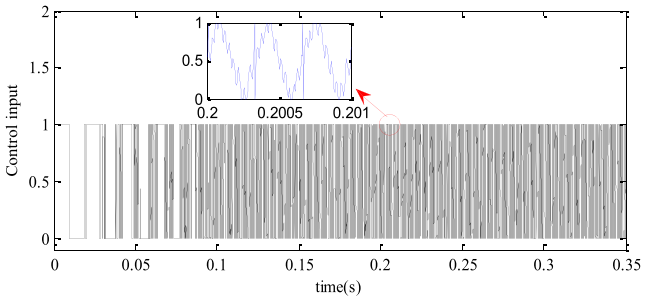

FIGURE 19. Control input using DOBFSMC.

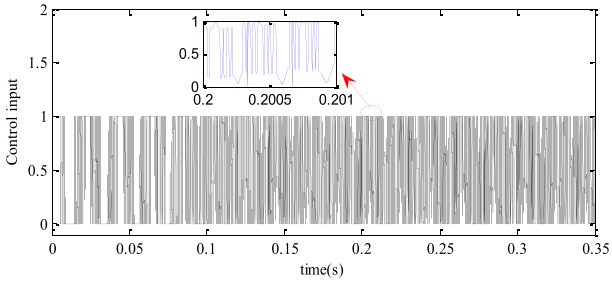

FIGURE 20. Control input using SMC.

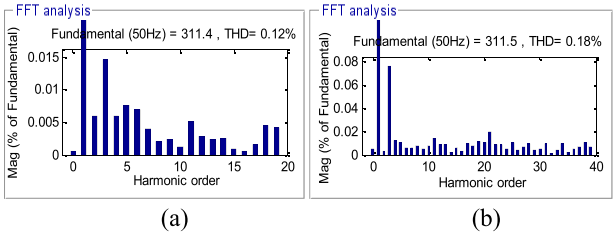

FIGURE 21. FFT analysis of inverter output voltage. (a) DOBFSMC (b) SMC.

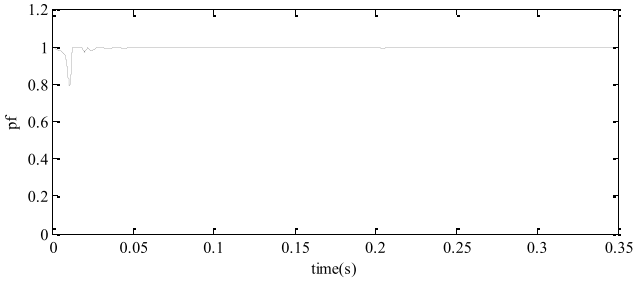

FIGURE 22. Power factor using DOBFSCM.

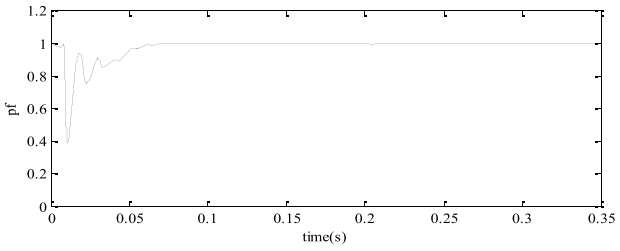

FIGURE 23. Power factor using SMC.

can keep consistent with the grid reference voltage with little error all the time, so the circulating current between the power supplies can be greatly reduced.

D. COMPARISON TO SMC

In order to prove the superiority of the proposed strategies, comparison with the ordinary SMC is accomplished under the conditions of load and parameter variations and environmental changes.

Voltage tracking properties shown in Fig.17 and Fig.18 demonstrate that the output voltage of inverter using the two strategies can both track the grid reference voltage very quickly. In the dynamic process, the output of inverter using DOBFSMC is synchronized with the reference voltage in phase although it has not yet tracked the reference voltage, however there is a phase difference between the inverter output voltage and the reference voltage using the SMC scheme in dynamic process. From the error curve, it can be seen that the tracking error using the two schemes can both converge gradually, but the error amplitude of the proposed method is bounded by $|e| < 0.8$ while that of SMC is $|e| < 3.2$, which is four times of the proposed method.

The control input when using SMC shown in Fig.20 has significant jump because SMC introduces a large switching term to compensate the impact of the uncertain disturbance. However, as shown in Fig.19, the control input of the proposed strategy is much smoother since the switching gain in sliding mode control is greatly reduced for designing a disturbance observer to compensate the disturbance and a fuzzy system to estimate the upper bound of the error between the observer output and the actual disturbance.

Fig.21 shows the FFT analysis of the two strategies, the THD of SMC is higher than that of proposed strategy in steady state indicating that the proposed scheme has better voltage quality. Furthermore, the power factor of SMC in the dynamic process is much lower than that of OBFSMC as can be seen in Fig.22 and Fig.23, the power factor of the proposed strategy can reach unity in a very short period of time. In summary, the simulation results above prove the superiority of the proposed strategy in both dynamic progress and steady state than SMC.

VI. CONCLUSION

This paper presents a DOBFSMC strategy for the single-phase PV grid-connected inverter by controlling the duty cycle of the power switches of H-bridge. In the fact that the disturbances caused by the inverter parameter variations and changes of climatic conditions may seriously affect the control performance of the inverter, a disturbance observer is designed to estimate these system uncertainties in real time. A sliding mode controller with Lyapunov theorem based control law that designed with the output information of the disturbance observer is employed to control the output voltage of the DC-AC inverter, a fuzzy system is used to approximate the upper bound of the observation error between the actual disturbance and its observation value in order to improve the performance of the control system. Simulation results show that the proposed control strategy can work reliably under different conditions with high power factor and low THD. Comparisons with SMC prove the superiority of the proposed strategy.

REFERENCES

[1] L. V. S. Kumar and G. V. N. Kumar, "Power conversion in renewable energy systems: A review advances in wind and PV system," *Int. J. Energy Res.*, vol. 41, no. 2, pp. 182–197, 2017.

[2] R.-J. Wai and W.-H. Wang, "Grid-connected photovoltaic generation system," *IEEE Trans. Circuits Syst. I, Reg. Papers*, vol. 55, no. 3, pp. 953–964, Apr. 2008.

[3] H. Jedtberg, A. Pigazo, M. Liserre, and G. Buticchi, "Analysis of the robustness of transformerless PV inverter topologies to the choice of power devices," *IEEE Trans. Power Electron.*, vol. 32, no. 7, pp. 5248–5257, Jul. 2017.

[4] H. F. Xiao, L. Zhang, and Y. Li, "A zero-voltage-transition HERIC-type transformerless photovoltaic grid-connected inverter," *IEEE Trans. Ind. Electron.*, vol. 64, no. 2, pp. 1222–1232, Feb. 2017.

[5] E. Koutroulis, K. Kalaitzakis, and N. C. Voulgaris, "Development of a microcontroller-based, photovoltaic maximum power point tracking control system," *IEEE Trans. Power Electron.*, vol. 16, no. 1, pp. 46–54, Jan. 2001.

[6] C. Li, Y. Chen, D. Zhou, J. Liu, and J. Zeng, "A high-performance adaptive incremental conductance MPPT algorithm for photovoltaic systems," *Energies*, vol. 9, no. 4, p. 288, 2016.

[7] S. Mohanty, B. Subudhi, and P. K. Ray, "A grey wolf-assisted perturb & observe MPPT algorithm for a PV system," *IEEE Trans. Energy Convers.*, vol. 32, no. 1, pp. 340–347, Mar. 2017.

[8] F. Evran, "Plug-in repetitive control of single-phase grid-connected inverter for AC module applications," *IET Power Electron.*, vol. 10, no. 1, pp. 47–58, Jan. 2017.

[9] F. Xiao, L. Dong, S. F. Khahro, X. Huang, and X. Liao, "A smooth LVRT control strategy for single-phase two-stage grid-connected PV inverters," *J. Power Electron.*, vol. 15, no. 3, pp. 806–818, 2015.

[10] C. Cecati, F. Ciancetta, and P. Siano, "A multilevel inverter for photovoltaic systems with fuzzy logic control," *IEEE Trans. Ind. Electron.*, vol. 57, no. 12, pp. 4115–4125, Dec. 2010.

[11] W.-H. Chen, "Disturbance observer based control for nonlinear systems," *IEEE/ASME Trans. Mechatronics*, vol. 9, no. 4, pp. 706–710, Dec. 2004.

[12] H.-S. Kim and K.-H. Kim, "Voltage-sensorless control scheme for a grid connected inverter using disturbance observer," *Energies*, vol. 10, no. 2, p. 166, 2017.

[13] E. Ozsoy *et al.*, "Control strategy for a grid-connected inverter under unbalanced network conditions—A disturbance observer-based decoupled current approach," *Energies*, vol. 10, no. 7, p. 1067, 2017.

[14] A. Sabanovic, "Variable structure systems with sliding modes in motion control—A survey," *IEEE Trans. Ind. Informat.*, vol. 7, no. 2, pp. 212–223, May 2011.

[15] X. Chen, J. H. Park, J. Cao, and J. Qiu, "Sliding mode synchronization of multiple chaotic systems with uncertainties and disturbances," *Appl. Math. Comput.*, vol. 308, pp. 161–173, Sep. 2017.

[16] X. Chen, J. H. Park, J. Cao, and J. Qiu, "Adaptive synchronization of multiple uncertain coupled chaotic systems via sliding mode control," *Neurocomputing*, vol. 273, pp. 9–21, Jan. 2018.

[17] S. Dhar and P. K. Dash, "A new backstepping finite time sliding mode control of grid connected PV system using multivariable dynamic VSC model," *Int. J. Elect. Power Energy Syst.*, vol. 82, pp. 314–330, Nov. 2016.

[18] V. F. Pires, J. F. Martins, and C. Hao, "Dual-inverter for grid-connected photovoltaic system: Modeling and sliding mode control," *Solar Energy*, vol. 86, no. 7, pp. 2106–2115, Jul. 2012.

[19] A. Menadi, S. Abdeddaim, A. Ghamri, and A. Betka, "Implementation of fuzzy-sliding mode based control of a grid connected photovoltaic system," *ISA Trans.*, vol. 58, pp. 586–594, Sep. 2015.

[20] A. Merabet, L. Labib, A. M. Y. M. Ghias, C. Ghenai, and T. Salameh, "Robust feedback linearizing control with sliding mode compensation for a grid-connected photovoltaic inverter system under unbalanced grid voltages," *IEEE J. Photovolt.*, vol. 7, no. 3, pp. 828–838, May 2017.

[21] N. Kumar, T. K. Saha, and J. Dey, "Sliding-mode control of PWM dual inverter-based grid-connected PV system: Modeling and performance analysis," *IEEE J. Emerg. Sel. Topics Power Electron.*, vol. 4, no. 2, pp. 435–444, Jun. 2016.

[22] J. Fei and Y. Zhu, "Adaptive fuzzy sliding control of single-phase PV grid-connected inverter," *PLoS ONE*, vol. 12, no. 8, p. e0182916, 2017.

[23] Y. Zhu and J. Fei, "Adaptive global fast terminal sliding mode control of grid-connected photovoltaic system using fuzzy neural network approach," *IEEE Access*, vol. 5, pp. 9476–9484, 2017.

[24] M. Rezkallah, S. K. Sharma, A. Chandra, B. Singh, and D. R. Rousse, "Lyapunov function and sliding mode control approach for the solar-PV grid interface system," *IEEE Trans. Ind. Electron.*, vol. 64, no. 1, pp. 785–795, Jan. 2017.

[25] W.-H. Chen, D. J. Ballance, P. J. Gawthrop, and J. O'Reilly, "A nonlinear disturbance observer for robotic manipulators," *IEEE Trans. Ind. Electron.*, vol. 47, no. 4, pp. 932–938, Aug. 2000.

[26] J. Fei and C. Lu, "Adaptive sliding mode control of dynamic systems using double loop recurrent neural network structure," *IEEE Trans. Neural Netw. Learn. Syst.*, vol. 29, no. 4, pp. 1275–1286, Apr. 2018.

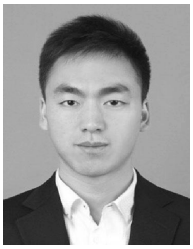

YUNKAI ZHU received the B.S. degree in electrical engineering from Hohai University, China, in 2015, where he is currently pursuing the M.S. degree in electrical engineering. His research interests include power electronics, adaptive control, and intelligent control.

JUNTAO FEI (M'03–SM'14) received the B.S. degree in electrical engineering from the Hefei University of Technology, China, in 1991, the M.S. degree in electrical engineering from the University of Science and Technology of China in 1998, and the M.S. and Ph.D. degrees in mechanical engineering from The University of Akron, OH, USA, in 2003 and 2007, respectively. He was a Visiting Scholar with the University of Virginia, VA, USA, from 2002 to 2003. He was a Post-Doctoral Research Fellow and an Assistant Professor with the University of Louisiana, LA, USA, from 2007 to 2009. He is currently a Professor with Hohai University, China. His research interests include adaptive control, nonlinear control, intelligent control, the dynamics and control of MEMS, and smart materials and structures.